Phosphotungstic acid-enhanced microcomputed tomography for quantitative visualization of mouse mammary gland morphology

Anthi Kolokotroni,[a,b] Evi Gkikopoulou,[a,b] Vagelis Rinotas,[b] and Eleni Douni[a,b,*]

[a]Agricultural University of Athens, Department of Biotechnology, Laboratory of Genetics, Athens, Greece

[b]Biomedical Sciences Research Center "Alexander Fleming," Institute for Bioinnovation, Vari, Greece

Abstract

Purpose: Even though current techniques provide two-dimensional (2D) imaging of the mouse mammary gland, they fail to achieve high-resolution three-dimensional (3D) reconstruction and quantification. The objective of this study is to establish and evaluate quantitative visualization of the mouse mammary epithelium through microcomputed tomography (microCT) using phosphotungstic acid (PTA) as a contrast agent.

Approach: *Ex vivo* microCT scan images of the mouse mammary glands were obtained following staining by PTA, whereas for quantification we adapted volumetric parameters that are used for assessing trabecular bone morphometry and can be structurally applicable in the mammary ductal system. The proposed method was validated in distinct developmental stages and upon short-term treatment with synthetic progesterone, using the carmine alum staining for comparison.

Results: We demonstrate a simple PTA staining procedure that allows high contrast 3D imaging of mammary glands and quantitation of mammary duct structures using microCT. We validated the proposed method in distinct developmental stages, such as at puberty, adult mice, pregnancy as well as upon progesterone treatment. Compared with carmine alum staining, the microCT analysis provided higher resolution 2D and 3D images of the mammary gland morphology, with lower background that enabled the detection of subtle changes.

Conclusions: This work is the first study that employs PTA-enhanced microCT for 3D imaging and volumetric analysis of mouse mammary glands. Our results establish PTA-enhanced microCT as a useful tool for comparative studies of the mouse mammary gland morphology that can apply in mutant mice and for the preclinical evaluation of pharmaceuticals in breast cancer models.

 [DOI: 10.1117/1.JMI.10.S2.S22402]

Keywords: mouse mammary gland; three-dimensional imaging; microcomputed tomography; phosphotungstic acid; contrast agent.

Paper 22210SSR received Aug. 10, 2022; accepted for publication Dec. 20, 2022; published online Feb. 21, 2023.

1 Introduction

The mammary gland is a highly dynamic organ that undergoes extensive remodeling in the epithelium starting from puberty and continuing throughout the reproductive cycle. The mammary gland epithelium forms a tree of ducts that consists of two cell layers, an inner layer of luminal cells that is surrounded by an outer layer of myoepithelial cells adjacent to a basement

*Address all correspondence to Eleni Douni, douni@aua.gr; douni@fleming.gr

2329-4302/2023/$28.00 © 2023 SPIE

membrane. The ductal tree invades into the stromal compartment composed of adipocytes, vascular endothelial cells, fibroblasts, and immune cells. At birth, the mouse mammary ductal tree is rudimental while elongation starts around 4 weeks of age, when ovarian hormones stimulate the development of terminal end buds (TEBs) at the tips of growing ducts.[1] Proliferation of TEB cells leads to the bifurcation and elongation of the ductal tree towards the outer edges of the fat pad by 10 to 12 weeks of age, when the TEBs regress and the mammary epithelium undergoes cycles of ductal side-branching in each estrous cycle in response to hormonal changes. During pregnancy, a massive mammary tissue remodeling results in the formation of the secretory alveoli from the luminal epithelial cells, which synthesize and secrete milk during lactation, whereas the contraction of the myoepithelial cells facilitates the excretion of milk from the mammary gland. The mammary gland returns into a prepregnancy state through the stage of involution, characterized by the regression of the lactating epithelium due to programmed cell death.[2] Progesterone is considered the major regulator of ductal side-branching and alveologenesis during pregnancy, inducing mitotic effects on mammary epithelial cells through two distinct waves of proliferation. The first autocrine wave affects progesterone receptor (PR) positive (PR^+) cells, and depends on the expression of the cell cycle regulator Cyclin D1, while a second larger paracrine wave targets PR negative (PR^-) cells and is mediated by the secretion of the cytokine receptor activator of nuclear factor kappa-B ligand (RANKL).[3–5] Due to similarities with the human breast, the mouse mammary gland has been widely studied for understanding the pathophysiology of the mammary gland, including the development of breast cancer.[6] However, the imaging techniques that are available for the analysis of the mouse mammary gland fail to provide high-resolution three-dimensional (3D) reconstruction and quantification.

Various techniques have been established to monitor and visualize *ex vivo* the development of the mammary gland at a two-dimensional (2D) level. Hematoxylin and eosin (H/E) staining of tissue sections allows evaluation of distinct cytoplasmic, nuclear, or extracellular compartments, and constitutes the gold standard of histopathological diagnosis for more than 100 years, detecting tissue alterations to grade tumor and guide clinical decision.[7,8] However, it is challenging to achieve 3D reconstruction of the entire mammary gland with H/E, as it requires multiple sequential paraffin sections assisted by computer-aided image analysis, even though thick section histopathology helps 3D imaging.[9] Recent studies attempted 3D reconstructions of mammary glands using alignment algorithms for piling serial sections of paraffin-embedded glands,[10–12] while measurements largely rely on 2D projections.

Whole mounting is a well-established method, frequently used for the assessment of the rodent mammary glands, as it can detect various morphological features or abnormalities. Whole mount staining with carmine alum, a nuclear stain, allows detection of epithelial structures embedded in the adipose tissue of the fat pad and is used for 2D image analysis that offers quantitative assessment of mammary gland density and side-branching.[13–17] Moreover, whole mount immunostaining and consequently optical projection tomography were also used to reconstruct 3D images for visualization of the mammary glands, whereas quantitative analysis was performed again from 2D images.[18] However, the true shape of a 3D object can be determined only using 3D imaging techniques. It is, hence, important to develop 3D quantitative methods equipped with a resolution capacity of high sensitivity. X-ray phase-contrast tomography is an emerging 3D label-free imaging technique that has been applied to detect breast cancer with higher spatial resolution and lower radiation doses than the 2D radiographies used in clinics today.[19,20]

Microcomputed tomography (microCT) is an x-ray imaging method that provides 3D high-resolution imaging of mineralized animal tissues and is currently the gold standard for the quantification of trabecular and cortical bone microstructure in small animal models.[21] However, a considerable limitation of this technology is the low intrinsic x-ray contrast of non-mineralized tissues, that prevents the microCT imaging of soft tissues in preserved animal specimens. Various contrast enhancing agents have been examined for soft tissue visualization through microCT, including iodine that easily penetrates into soft tissues offering high contrast, although it usually causes severe soft tissue shrinkage.[22,23] Moreover, osmium tetroxide (OsO_4), a well-known reagent that binds specifically to unsaturated lipids, has been recently used for the 3D visualization of bone marrow adipose tissue and the quantification of its amount and distribution in long

bones of mice using microCT.[24] Phosphotungstic acid (PTA) is an alternative staining agent recently used as a contrast agent for x-ray techniques, because it contains tungstic ions that bind to basic groups of proteins and connective tissue, whereas at the same time tungsten is a metal with high atomic number. Staining of proteins with PTA is a predominantly electrostatic interaction because PTA anions bind to positively charged amino acid side-chains. Due to the abundance of lysine and arginine in collagen, PTA binds strongly to collagen, which is the major structural protein in a variety of tissues.[25] Moreover, PTA-hematoxylin staining is used to detect fibrin deposits in tissue lesions[26] and glial fibers in reactive astrocytes of the neural tissue.[27] The PTA staining has been already successfully applied for high-resolution microCT imaging of various animal specimens such as insects, chicken and mouse embryos, mouse ovaries, hearts, and kidneys providing excellent contrast among different tissues.[28–32] Recently, PTA contrast enhanced microCT offered high-resolution 3D visualization of pathological alterations in the murine kidney such as renal fibrosis.[33] Thus, development of microCT-based techniques could provide 3D imaging of soft tissues such as the mammary gland.

In the current study, for the first time we present a method of 3D visualization of the mouse mammary glands through PTA contrast enhanced microCT. Based on our expertise on microCT imaging and quantification of the bone parameters in mouse models of bone diseases,[34,35] we here propose to measure and count mammary ductal tree structures using parameters widely used for trabecular bone analysis with microCT.[21] We validated the proposed method in distinct developmental stages such as at puberty, mature adults, pregnancy as well as upon progesterone treatment. In addition, we compared PTA-enhanced microCT with the 2D whole mount carmine alum staining. This technique can be applied for 3D high-resolution analysis of the mouse mammary gland morphology during normal development, precancer and cancer lesions as well as upon preclinical treatments.

2 Methodology

2.1 *Mouse Maintenance and Treatment*

C57BL/6 female mice were maintained and bred in the animal facility of the Biomedical Sciences Research Center "Alexander Fleming" (EL09BIO05) under specific pathogen-free conditions. All experimental protocols were performed with the approval of the Institutional Protocol Evaluation Committee and were licensed by the Veterinary Authorities of Attica Prefecture (533/13-02-2019) in compliance with the animal welfare guidelines of the PD 56/2013 and the European Directive 2010/63/EU. Medroxyprogesterone acetate (MPA) (Sigma Aldrich) was diluted in cottonseed oil (10% DMSO) and was administered orally at a dosage of 25 mg/kg for 4 consecutive days in 8-week-old C57BL/6 female mice. Diluent solution (10% DMSO diluted in cottonseed oil) was administered in control mice ($n = 6$ per group).

2.2 *Carmine Alum Staining of Mammary Glands*

Whole mounts of abdominal mammary glands were stained with carmine alum as previously reported with some modifications.[13–17] Briefly, mammary glands were spread on a glass slide and were left to dry for 1 min before they were fixed in 4% formalin at 4°C overnight. The next day, the mammary glands were washed with 70% ethanol for 15 min followed by hydration by short rinse in 50% ethanol (5 min) and then in water. Alternatively, the tissues can be stored in 70% ethanol until staining. Mammary glands were stained in carmine alum solution containing 0.2% of Carmine (Sigma-Aldrich) and 19.36 mM of aluminum potassium sulfate (Acros Organics) for 6 days depending on the thickness of the mammary fat pad. After wash with water and gradual dehydration with serial dilutions of ethanol (70% overnight, 95% and 100% for 1 hour each), they were immersed and stored in xylene for 3 to 6 days, depending on the thickness of the mammary fat pad, until mounting with glycerol. The protocol process is schematically presented in Fig. 1(a).

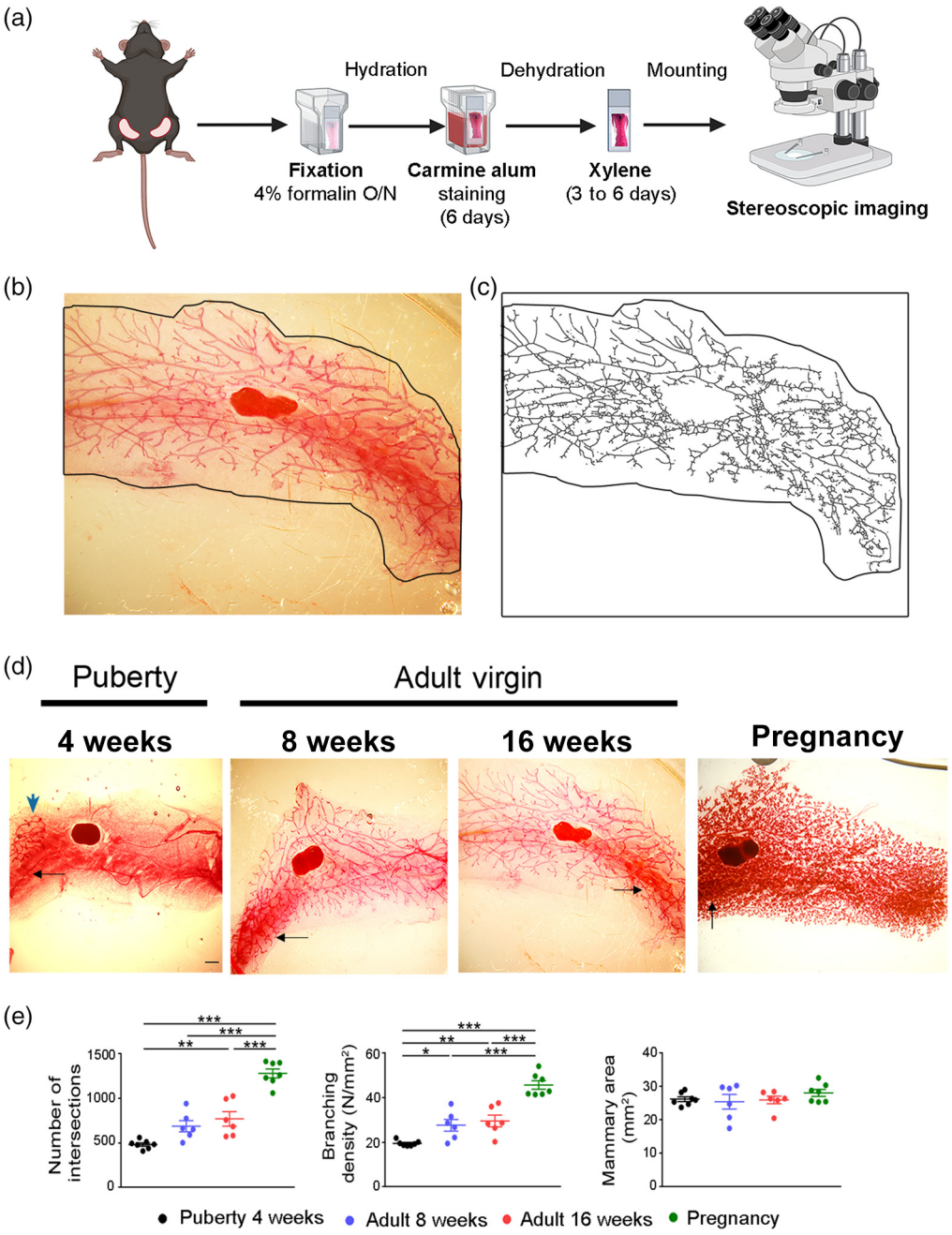

Fig. 1 Imaging and semiquantification of mammary gland epithelium stained with carmine alum. (a) Schematic overview of the procedure followed for carmine alum staining of the mammary glands. Created with BioRender.com. (b) Representative whole mount carmine alum staining and (c) its skeletonized image that was used to perform Sholl analysis in an abdominal mammary gland from an 8-week-old virgin C57BL/6 mouse. Black outline defines the boundaries of the mammary fat pad. (d) Representative images of whole mounts of abdominal mammary glands stained with carmine alum at different stages (4, 8, and 16 weeks and pregnancy at 15.5 dpc). The high background is shown with black arrows, whereas the rudimentary duct at puberty by blue arrow. Scale bar = 1 mm, magnification = 2×. (e) Quantitative analysis of intersection number, branching density and mammary fat pad area at the distinct developmental stages through Sholl analysis ($n = 6$ to 7 per group). Data are shown as mean values ± SEM, one-way ANOVA and Tukey post-hoc test was performed for statistical analysis (*$p < 0.05$, **$p < 0.01$, ***$p < 0.001$).

2.3 *Quantitative Assessment of Mammary Glands Using Whole Mount Carmine Alum Staining*

Quantitative analysis of abdominal mammary glands stained with carmine alum was performed as previously published.[15] Briefly, images of mammary glands stained with carmine alum were acquired using a SMZ800 Nikon stereoscope (1× objective lens) and were processed with ImageJ software (version 1.53c). Mammary epithelium was manually delimited and isolated from the rest of the image, whereas lymph nodes were excluded from the analysis. Color channels were separated, and the background was subtracted. Noise was removed at first automatically using the despeckle command tool and any persistent noise was further removed manually. Threshold was adjusted and the images were skeletonized, made binary and dilated before Sholl analysis (version 4.02) was applied. Processed images were constantly compared to the originals and any details missing were corrected manually. Through Sholl analysis, the total number of intersections ("*N*") and the branching density of the mammary gland area ("N/total mammary gland area) were measured. Total mammary gland area was delimited manually and was estimated with ImageJ ("measure" command).

2.4 *PTA Staining of Mammary Glands*

PTA was dissolved in water to prepare 1% (w/v) PTA stock solution, which was diluted with absolute ethanol in a ratio 3:7 to prepare the 0.3% PTA working solution.[28,29] The mammary glands were pinned in a cork strip and submerged in a conical tube containing 4% formalin for up to 16 hrs at 4°C. Next day, the glands were washed thoroughly with water for at least one min to remove the fixation buffer and were stained with 0.3% PTA solution for 6 days with an intermediate change. After PTA staining, glands were immersed into 70% ethanol solution until microCT scanning. The protocol we established is schematically presented in Fig. 2(a). All samples were scanned within a week.

2.5 *MicroCT Scanning, Reconstruction, and Quantitative Analysis*

The mammary gland was stabilized with a pin on a piece of expanded polystyrene (styrofoam) and was placed into a microCT polypropylene tube containing 70% ethanol (Fig. S1 in the Supplementary Material). The tube was firmly stuck with a gum cap into the chuck supplied with the microCT scanner. The microarchitecture of the mouse mammary gland was analyzed using a high-resolution SkyScan1172 microtomographic imaging system (Bruker). The scanning conditions were 55 KV, 100 μA, camera binning 2×2, rotation step 0.4, 10 μm voxel size with a 0.5-mm aluminum filter to remove the undesirable x-rays with low energy. Scanning period was around 40 min per sample. Micro-CT reconstructed images were acquired in 8-bit bmp format (2000×1332 pixels) and the reconstruction process was performed automatically directly after the scan by the CT-specific software Nrecon (version 1.7.4.6), using beam hardening correction, ring reduction and misalignment compensation. The mammary gland region that was analyzed comprised about 7.225-mm (850 microCT image slices) covering ~80% of the total mammary fat pad area including the lymph node. Each time segmentation of microCT images was performed, applying an appropriate threshold value with the condition that the binarized images of the mammary epithelium resembled with accuracy the original images. Image processing steps such as despeckling were applied to remove noise dots. 2D and 3D microCT representative images were acquired by CTan (version 1.18.8.0+) and CTvol (version 2.3.2.0) software, respectively. For quantitation of the mammary duct morphology, we selected and adapted parameters that are classically used for trabecular bone analysis with microCT (Table S1 in the Supplementary Material),[21] including ductal volume (DV, mm^3), DV/tissue volume (DV/TV, %), ductal separation (D.Sp, mm), ductal thickness (D.Th, mm), number of ducts (D.N, mm^{-1}), ductal surface (DS, mm^2), DS density (DS/TV, mm^{-1}), and fractal dimension (FD). Data are shown as mean values ± standard error of the mean (SEM).

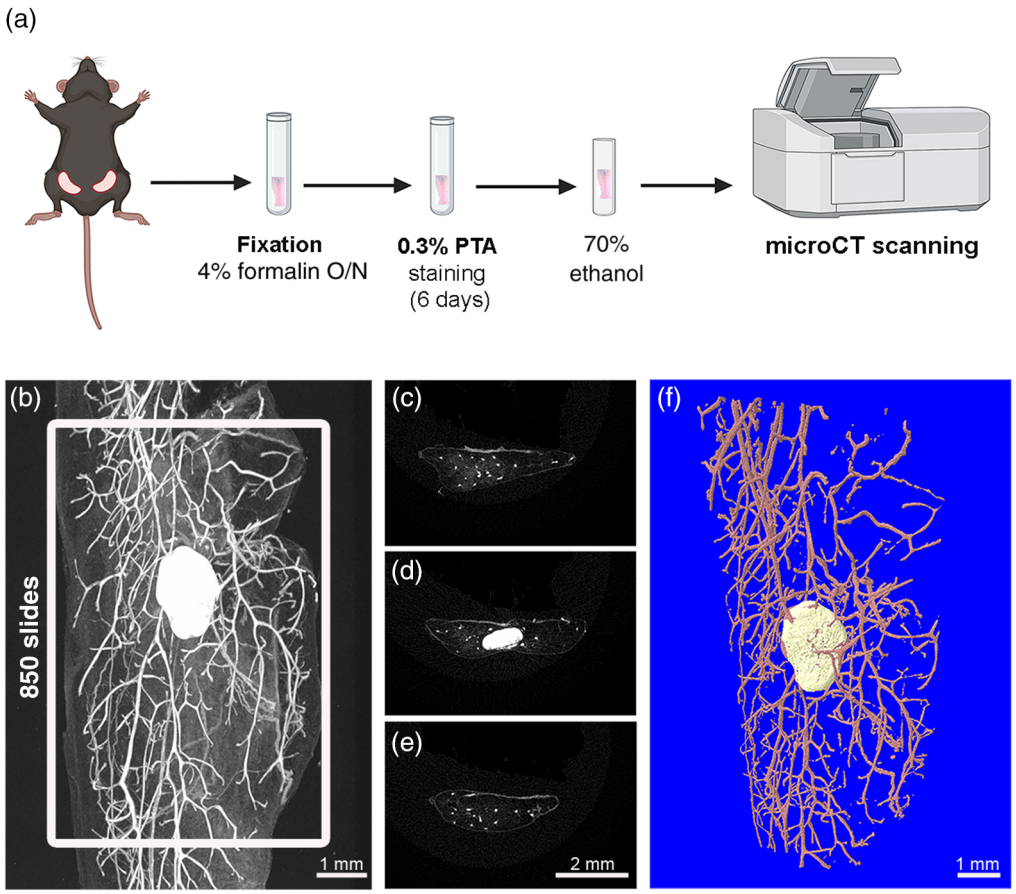

Fig. 2 2D and 3D imaging of mouse mammary gland with PTA-enhanced microCT. (a) Schematic overview of PTA staining protocol and subsequent microCT scanning of abdominal mammary gland tissue. Created with BioRender.com. (b) Acquisition of 2D representative microCT image of mammary gland after PTA staining using CTan software. White frame illustrates the area of interest containing 850 contiguous slides including the lymph node. (c–e) Transverse sections of mammary gland from proximal to distal regions showing ductal epithelium as white spots and lymph node in panel D. (f) 3D reconstructed image of the mammary ductal tree (pink) and lymph node (beige) using CTvol software (Bruker).

2.6 *Quantitative Real-Time PCR (qPCR) Expression Analysis*

Total RNA was extracted from abdominal mammary glands using a monophasic solution of guanidine isothiocyanate and phenol according to the manufacturer's instructions (TRI Reagent, MRC). After removal of DNA remnants with DNase I treatment (Sigma-Aldrich), first-strand cDNA was synthesized using 2 μg of total RNA and M-MLV (Invitrogen). Templates were amplified with EvaGreen Master Mix (Solis Biodyne) on the CFX96 Connect real time PCR instrument (Bio-Rad Laboratories). Data analysis was following the $2^{-\Delta\Delta CT}$ method. A pair of primers (Eurofins Genomics) specific for the cyclin D1 (CCD1) gene was used for qPCR analysis (F: 5′-GCGTACCCTGACACCAATCTC-3′ and R: 5′-CTCCTCTTCGCACTTCTG CTC-3′). The PCR was performed in a 20-μl reaction using 58°C as the annealing temperature for 40 cycles. PCR using primers specific to the β-2 microglobulin gene (5′-TTC TGG TGC TTG TCT CAC TGA-3′ and 5′-CAG TAT GTT CGG CTT CCC ATT C-3′) was also carried out as an internal control, using the same RNA samples and same conditions. Five biological and two technical replicates were used.

2.7 *Histological Analysis and Immunostaining*

Mammary glands were isolated and fixed with 4% paraformaldehyde (PFA) in phosphate-buffered saline (PBS) overnight at 4°C. The glands were subsequently embedded in paraffin

and 5-μm sections were obtained. For histological analysis, tissue sections were stained with hematoxylin and eosin (H/E), and histology images were acquired using a Nikon E800 upright widefield/fluorescence microscope (10× objective lens). For immunofluorescence (IF), mammary sections were deparaffinized in xylene and subsequently hydrated in serial ethanol solutions from 100% to 50%. Permeabilization was carried out with 0.5% Triton in PBS for 30 min and endogenous peroxidase activity was inhibited with 3% H_2O_2 for 10 min. Mammary gland sections were then incubated with a blocking solution containing 2% BSA and 1.5M Glycine in PBS for 1h at room temperature. The following primary antibodies were used at indicated dilutions for overnight incubation at 4°C: monoclonal rabbit anti-Cytokeratin 8 at 1:250 (Abcam, ab53280) and monoclonal rabbit anti-Cyclin D1 at 1:250 (Abcam, ab134175). Mammary specimens were washed with PBS and were incubated with fluorescently tagged secondary antibodies (Jackson ImmunoResearch) against the appropriate species (diluted 1:1000) for 1 hr at room temperature. After three washes with PBS the mammary gland sections were mounted with DAPI (Biotium). IF images were acquired using a Leica DM2000 Fluorescent Microscope (10× objective lens) and were analyzed with the ImageJ and IHC toolbox plugin as previously published.[36]

2.8 *Statistical Analysis*

All results were represented as scatter dot-plot showing each data point, as mean values ± SEM. Statistical comparisons were performed by one-way analysis of variance (ANOVA) and Tukey posthoc test to compare means of multiple groups. Unpaired t-test analysis was carried out to compare two groups. For all tests, $p < 0.05$ was considered statistically significant.

3 Results

3.1 *2D Imaging of Whole Mount Mammary Glands Stained with Carmine Alum*

Different developmental stages of abdominal mammary glands were assessed with whole mount carmine alum staining and measurement of the ductal branching density was performed using the Sholl analysis method[15,17] based on the skeletonized images [Figs. 1(b) and 1(c)]. Abdominal mammary glands were selected due to their clear structure and the absence of muscle impurities. As expected, mammary glands from 4-week-old females formed a rudimentary duct which is restricted to the distal region of the fat pad, whereas at 8 and 16 weeks, an extended network of epithelial ducts was spread throughout the fat pad area [Fig. 1(d)]. At pregnancy (15.5 dpc), mammary glands displayed structural alterations due to alveologenesis [Fig. 1(d)]. However, our assessment of the mammary ductal branching density encountered technical difficulties mostly due to the heterogenous staining and the high background observed usually at areas of high complexity [Fig. 1(d)]. Nevertheless, our measurements confirmed that from puberty (4-week-old) to pregnancy there is a progressive increasing number of ductal branching (4 weeks: 483 ± 19; 8 weeks: 688 ± 63; 16 weeks: 770 ± 81; and pregnancy: 1280 ± 49) and branching density (4 weeks: 19.51 ± 0.47; 8 weeks: 27.66 ± 2.61; 16 weeks: 29.58 ± 6.40; and pregnancy: 45.72 ± 1.90), whereas the total mammary fat pad area among all examined groups was similar [Fig. 1(e)]. In conclusion, whole mount carmine alum staining provided a 2D imaging of the mammary ductal tree expansion during the various developmental stages, whereas quantification of ductal branches was affected by the heterogeneous background and the high complexity during pregnancy.

3.2 *3D Imaging of Mammary Glands Through PTA-Enhanced MicroCT*

Considering the complexity of the mammary gland and the limitations associated with the 2D analysis of carmine-stained specimens, we investigated the application of PTA-enhanced microCT for the 3D imaging of the mouse mammary ductal tree and the quantification of various mammary epithelial parameters. Because PTA has been previously applied for the visualization

of soft tissues with microCT,[28–31] we hypothesized that it could provide a strong signal at the mouse mammary ductal system compared with the surrounding adipose tissue. Our results demonstrated that utilizing PTA staining as a contrast enhancing reagent in microCT, was sufficient to detect effectively and at high-resolution of ~10 μm the ductal tree, the lymph nodes and blood vessels as depicted by the 2D shadow projection image of a mammary gland isolated from a 8-week-old C57BL/6 female [Fig. 2(b)]. Notably, the mammary adipose tissue, which is characterized by limited cytoplasm, was not stained by PTA and appeared dark in the 2D microCT rendering images. Setting a consistent volume of interest (VOI) in all mammary specimens is fundamentally important to obtain 3D imaging and comparative quantitative data. Thus, we set a VOI of 850 slices which covers most of the mammary gland area (~80% of total area) regardless of the developmental stage, including also the lymph node [Fig. 2(b)]. This enables capture of high-resolution images of the PTA-stained mammary epithelium as depicted both by longitudinal and transverse sections [Figs. 2(b)–2(e)]. Furthermore, within the mammary area, we set a region of interest (ROI) in every slice that includes mammary ducts and vessels but not the lymph node to quantify ductal parameters. In each mammary gland section, ROIs were manually drawn around the outer boundary of the fat pad, resulting in a 3D model of the mammary ductal tree that can be reconstructed utilizing CtAn and CtVol software [Fig. 2(f)]. This approach allowed 3D reconstruction of the mammary epithelium tree with high resolution.

3.3 *Quantitative Visualization of Mammary Gland Epithelium Through PTA-Enhanced MicroCT*

To compare the PTA contrast-enhanced microCT with the results obtained from carmine alum staining, we analyzed the mammary glands from mice of the same developmental stages such as nulliparous mice of 4-, 8-, and 16-week-old and pregnant mice at 15.5 dpc (Fig. 3). Abdominal mammary glands from all examined groups were stained with PTA and were scanned in microCT at resolution with a voxel size of 10 μm to obtain 2D and 3D images as described above [Figs. 3(a) and 3(b)]. Imaging of the abdominal mammary gland morphology from 4-week-old females (puberty) with microCT revealed that the mammary epithelium was rudimentary occupying limited space in the fatty parenchyma as shown at the upper part of the 2D and 3D images [Fig. 3(a)]. TEBs were evident at puberty as well, forming club-shaped structures at the tips of growing buds [Fig. 3(b)]. Moreover, the lymph node and the vessels were clearly depicted [Figs. 3(a) and 3(b)]. Mammary glands from 8- and 16-week-old virgin mice exhibited a well-organized ductal tree with branches throughout the fat pad [Figs. 3(a) and 3(b)]. Furthermore, 2D and 3D microCT images from mammary glands during pregnancy clearly displayed a dense network of alveolar structures, with formation of alveolar buds at the tips of ductal branches, as shown in high magnification [Fig. 3(b)].

Based on our expertise on the assessment of mouse bone microstructure with microCT,[34,35] we investigated whether we could adapt parameters widely used for trabecular bone analysis[21] for the quantitative analysis of mammary ductal tree structures (Table S1 in the Supplementary Material). We defined nine parameters that could be used to assess volumetric aspects of mammary epithelium, which were measured from the 3D reconstructed images [Figs. 3(a) and 3(b)]. Our analysis showed that the DV fraction progressively increased from puberty to adult mice while at pregnancy reached the highest values (DV/TV %, puberty: 1.63 ± 0.19, 8 weeks: 5.72 ± 0.45, 16 weeks: 4.37 ± 0.37, and pregnancy: 21.52 ± 1.72) [Fig. 3(c), Table S2 in the Supplementary Material]. Similarly, the estimated ductal number increased during the expansion of the mammary ductal tree, while the mammary D.Sp which indicates free space among the ductal branches was inversely related to the above parameters [Fig. 3(c), Table S2 in the Supplementary Material]. Furthermore, the average D.Th did not alter from puberty to adult stage but significantly increased at pregnancy [Fig. 3(c), Table S2 in the Supplementary Material]. The DS density as expressed by ductal surface/tissue volume (DS/TV, %) showed similar results with the DV/TV % among the various groups, confirming developmental differences in the mammary epithelium (puberty: 1.19 ± 0.14, 8 weeks: 3.58 ± 0.27, 16 weeks: 2.53 ± 0.22, and pregnancy: 9.04 ± 0.91). Finally, the FD parameter provided an estimation of the epithelium complexity reflecting the magnitude of ductal branching[37] [Fig. 3(c), Table S2 in the Supplementary Material]. Collectively, our results demonstrate that PTA-enhanced microCT

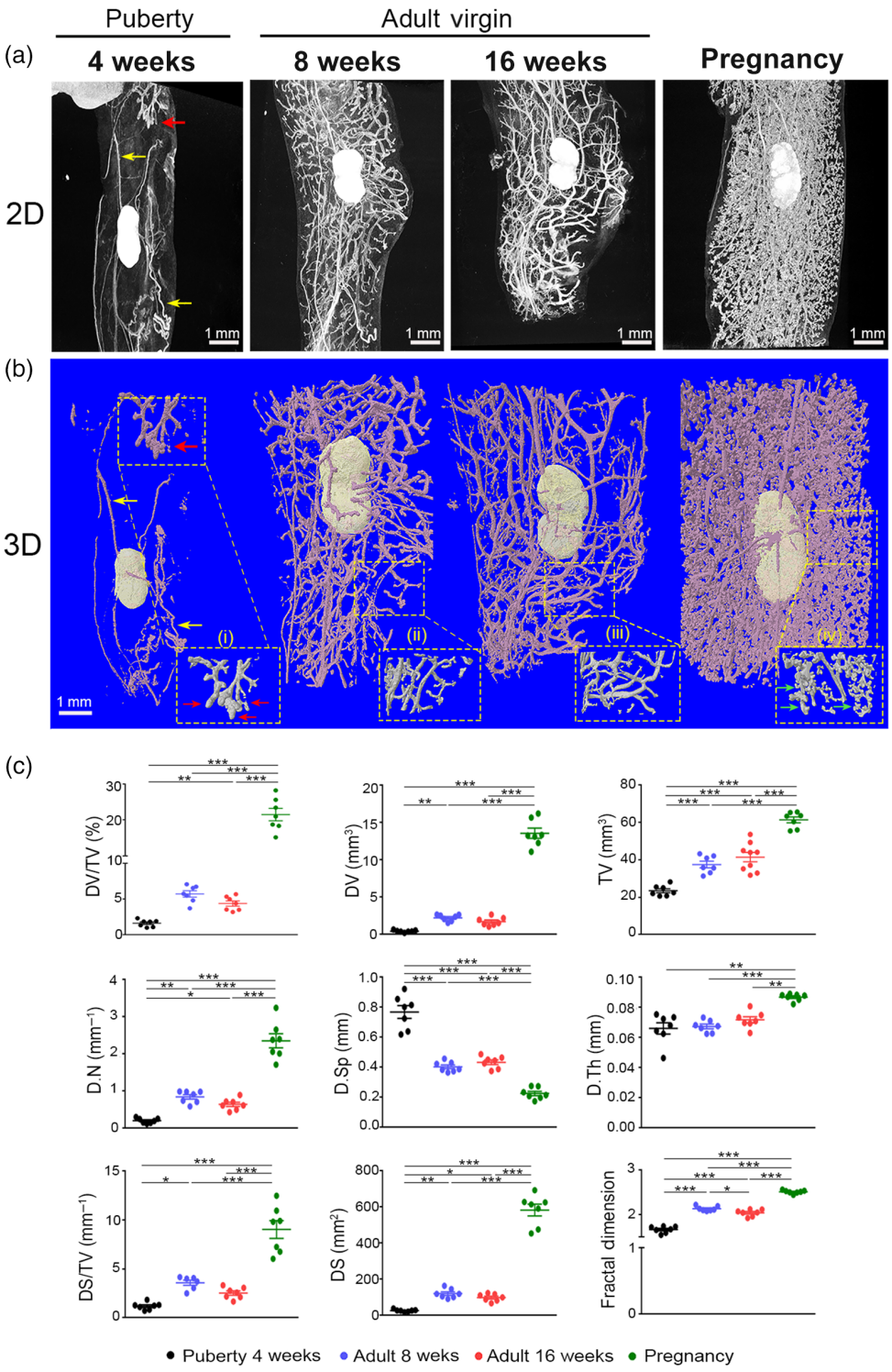

Fig. 3 3D imaging and quantification analysis of the abdominal mammary gland during distinct developmental stages with PTA-enhanced microCT. (a) Representative 2D microCT images and (b) 3D reconstruction images of the mammary ductal tree from puberty to adult virgin and pregnancy. Selected regions were magnified as shown by dashed line squares depicting (i) the formation of TEBs (showed by red arrows), (ii, iii) ductal elongation in mature mammary gland, and (iv) alveolar formation during pregnancy (showed by green arrows). Yellow arrows at 4 weeks show vessels. (c) Quantitative analysis of mammary epithelium during the four distinct developmental stages ($n = 7$ per group). Data are shown as mean values ± SEM. One-way ANOVA, and Tukey post-hoc test was performed for statistical analysis (*$p < 0.05$, **$p < 0.01$, ***$p < 0.001$).

constitutes a powerful method not only for high-resolution 3D imaging of the mouse mammary gland but enables the adaption of bone parameters into the mammary gland to effectively quantify mammary duct parameters for the estimation of the mammary density and the complexity of mammary epithelium. Compared with carmine staining, the microCT analysis provided higher resolution 2D and 3D images of the mammary gland morphology, whereas the background from the adipose tissue was minimal.

3.4 *Detection of Morphological Changes in Mammary Gland Epithelium upon MPA Treatment*

We further compared the two imaging techniques, such as carmine staining/Sholl analysis and PTA-enhanced microCT, upon short-term treatment of mice with synthetic progesterone (MPA), that is well known to promote the expansion of mammary gland epithelium through induction of Cyclin D1 (CCD1).[38,39] The MPA was administered daily at 25 mg/kg for 4 consecutive days in 8-week-old C57BL/6 females (Fig. 4). The effectiveness of MPA treatment in the mammary epithelium was confirmed by histology, qPCR expression analysis for Cyclin D1 and immunofluorescence for Cyclin D1 and the luminal cell marker cytokeratin 8 (CK8)[4,40] (Fig. S2 in the Supplementary Material).

2D imaging analysis of mammary glands with carmine alum staining failed to identify significant differences as regards ductal branching density between the two experimental groups [Figs. 4(a) and 4(b)]. On the contrary, high-resolution imaging with PTA-enhanced microCT revealed subtle structural changes of epithelium such as thickening of the mammary ducts [Figs. 4(c)–4(e)]. Quantitative analysis confirmed a significant increase of the D.Th in mice treated with MPA [wild-type (WT) control: 0.065 ± 0.002, MPA-treated: 0.078 ± 0.004, $p < 0.05$], as well as of the ductal volume (WT control: 1.41 ± 0.21, MPA-treated: 2.34 ± 0.34, $p < 0.05$). Interestingly, the FD parameter was also significantly increased reflecting increased ductal branching, something that was difficult to observe at the 2D or 3D images [Figs. 4(c)–4(e)]. These results indicate that PTA-enhanced microCT provides a high-resolution imaging of the mammary ductal epithelium that with the tissue parameters used allows comparative quantification and identification even of subtle tissue changes that were not possible to be captured by 2D imaging methods, such as carmine alum staining.

4 Discussion

To date, the combination of 2D imaging techniques, including whole mount carmine alum staining and H/E staining of paraffin sections remains the gold standard for structural analysis of mouse mammary glands.[8,9,15,17,37,41] Phase-contrast tomography is a promising x-ray-based 3D imaging technology that provides enhanced soft-tissue contrast and improved visualization of breast cancerous structures at reduced radiation doses.[19,20] This image modality is limited to synchrotron light sources. However, different approaches have managed to use conventional x-ray tube sources and to develop small-animal scanners, opening possibilities for the application of phase-contrast tomography in a preclinical setting.[42,43]

MicroCT is an emerging 3D imaging modality, offering high-resolution reconstruction and quantitative volumetric measurements of tissues with a complex and heterogeneous microstructure. Even though microCT is a widely accessible whole-volume scanning method, is mainly applied in mineralized tissues because soft tissues display low x-ray absorption. To overcome this limitation, compounds containing high atomic number elements that bind to soft tissues are recently used as contrast agents in contrast enhanced microCT.[44] The most broadly contrast stains used so far are iodine and PTA.[29] However, iodine has been reported to provide strong contrast only in specific tissues, whereas its most significant drawback is the induction of severe tissue shrinkage that affects tissue morphology upon microCT analysis.[31,45] The PTA is a larger molecule containing tungsten ions that provides a general stain as it binds to various proteins and connective tissue. In parallel, tungsten, a transition metal, is an ideal contrast agent for x-ray techniques, such as microCT. Moreover, solution in alcohol makes the effective molecular size of PTA smaller, improving its perfusion into tissues and cells.[46] So far, various PTA staining

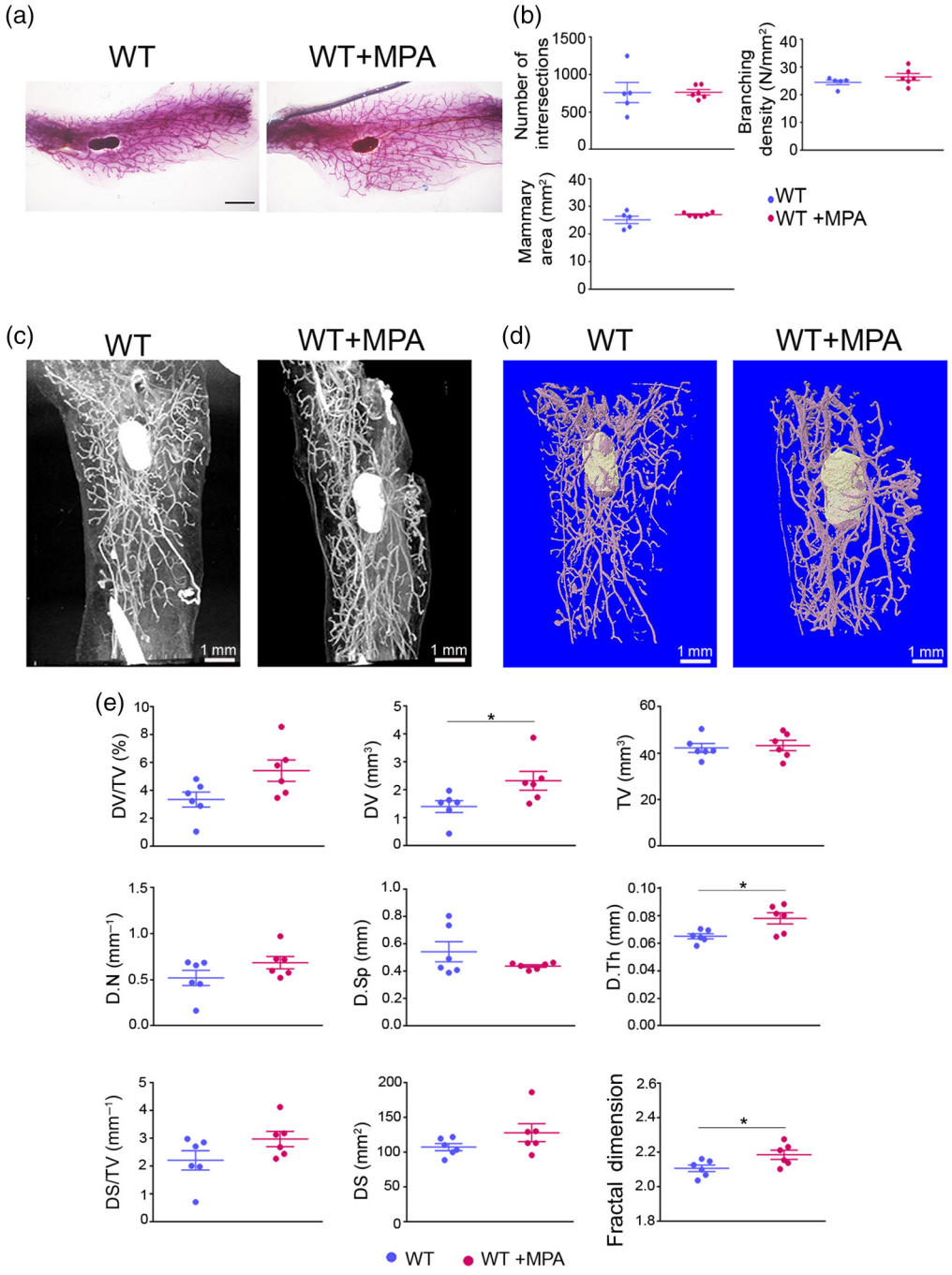

Fig. 4 Effect of short-term administration of MPA in the mammary glands. (a) Representative whole mount carmine alum staining images of abdominal mammary glands from MPA-treated and WT control female mice. Scale bar = 1 mm, magnification = 4×. (b) Semiquantitative analysis of intersection number, branching density and total mammary gland area using carmine alum staining, and Sholl analysis ($n = 5$ to 6 per group). (c) Representative 2D and (d) 3D reconstructed images through PTA-enhanced microCT of the mammary epithelium from MPA-treated and WT control mice. (e) Comparative quantitative analysis of mammary gland epithelium between MPA-treated and WT control mice employing PTA-enhanced microCT ($n = 6$). Data are shown as mean values ± SEM. Unpaired t-test was performed for statistical analysis (*$p < 0.05$).

protocols have been previously employed, which offer 3D visualization of the neuronal system, heart, liver, lungs, kidneys, ovaries, and mouse embryos.[28,30–33] It's worth mentioning that optimized PTA staining protocols preserve 3D morphology of soft tissues with minimal tissue shrinkage, whereas tissues can be subsequently analyzed by histological and immunohistochemical procedures.[30,31] In this study, we present a 3D imaging method for the visualization and volumetric analysis of the mammary ductal tree using PTA as contrast agent in microCT and we compare it with whole mount carmine alum staining. To the best of our knowledge, our approach is the first that provides high-resolution 3D visualization of *ex vivo* PTA-stained mammary glands through microCT.

Our results showed that staining of abdominal mammary glands with 0.3% PTA for 6 days was adequate for achieving complete tissue penetration, as shown by homogeneous contrast throughout the mammary gland in all developmental stages including pregnancy, where there is high epithelial tissue density and complexity. Similarly, other studies demonstrated high-contrast 3D images of animal soft tissues using 0.3% to 0.7% PTA staining solution with various staining durations depending on the tissue morphology and volume.[28,29,31,33] Because PTA binds to tissue proteins, it provides a 3D microstructure of the mammary ductal tree without noise from the surrounding adipose tissue. However, we cannot distinguish mammary ducts from the blood vessels since they have similar structure and average diameter [Fig. 3(a)]. Even though this cannot be avoided with the existing contrast stains, the interference of the vessel system in the ductal measurements is practically neglectable when the ductal system has reached the edges of the mammary fat pad and even more during pregnancy. Moreover, the microCT scanning period is around 40 min per sample to achieve a voxel size of 10 μm, enabling the scanning of multiple mammary glands within a day. To capture the 3D microstructure of the abdominal mammary gland specimens, we set a VOI of 850 slices, including the lymph node, which was utilized as a reference point [Fig. 2(b)]. For the quantitative analysis of mammary ductal tree structures, we adapted volumetric parameters that are classically used for the assessment of the trabecular bone morphometry through microCT, selecting variables that can be structurally applicable in the mammary ductal system.[21] Apart from the commercial software, there is also an open-source ImageJ plugin, BoneJ, that calculates trabecular parameters and could be used for mammary ductal analysis.[47] Moreover, further studies are needed to demonstrate whether microCT data could be processed through Sholl 3D analysis for the measurement of the number of intersections and branches as it has been previously reported for astrocytes using two-photon microscopy.[48]

To validate PTA as a contrast-enhancing staining agent in the mammary ductal tree, we assessed the morphology and performed volumetric analysis during four distinct developmental stages, such as week 4 (early puberty), week 8, and 16 (mature adults), and at pregnancy (15.5 dpc). At week 4, our 2D and 3D microCT imaging demonstrated the presence of a rudimentary ductal tree with TEBs, whereas at weeks 8 and 16, the ductal system was well implanted in the fat pad with numerous side branches without evidence of TEBs, as expected. At pregnancy, the complexity and the density of the ductal tree was increased due to formation of alveoli. These developmental changes were confirmed with the 2D images of carmine alum staining which, however, provided a heterogeneous background noise. Regarding the volumetric aspects of the analysis, during the maturation of the mammary ductal tree there was a progressive increase in the ductal volume (DV), the tissue volume (TV), and the ductal volume fraction (DV/TV%) that reached higher values at pregnancy, supporting the 3D imaging reconstructions [Fig. 3(c)]. Other parameters, such as ductal number, separation, and surface, collectively, also revealed significant differences among the various developmental stages, indicating a complex ductal network due to side branching at mature mammary glands that further increases at pregnancy due to alveologenesis. Our analysis also demonstrated that the D.Th significantly increased at pregnancy. The FD, a quantitative tool for objective measurement of complex structures, such as the ductal epithelium,[11,37] also demonstrated the progressive increase in the complexity of the ductal network from puberty to maturity and pregnancy.

The quantification of the 2D images from carmine alum–stained mammary glands relies on computer-assisted image analysis including the "Sholl analysis" plugin that is incorporated in ImageJ image processing package measuring mammary branching density in rodents.[15,17] Applying this quantification tool, we measured intersection number, branching density, and

mammary gland area in each developmental stage for comparison with our microCT volumetric results. Indeed, the first two parameters were lower at week 4 compared with mature mammary glands (weeks 8 and 16) and pregnancy, whereas they reached the highest values at pregnancy (Fig. 1). However, an important technical limitation of this approach is the heterogeneous staining of the mammary glands with carmine alum that leads to areas with high background in skeletonized images, which is difficult to be eliminated through automatic or manual interventions, especially at pregnancy where the ductal tree becomes even denser. Xiong et al.[49] (2020) managed to quantify various ductal parameters based on carmine alum–stained mammary glands only at 3 weeks of age, but not at 5 and 8 weeks due to high complexity. Instead, microCT analysis of PTA-stained mammary glands was superior compared with 2D carmine analysis due to minimal background from the surrounding fat pad and the high-resolution images that enabled the volumetric measurements. As a result, 3D measurements were feasible at all developmental stages that could demonstrate higher differences at the variables used. For example, comparing the mammary gland density between pregnancy and maturity (week 16), we identified a 5-fold increase with the volumetric fraction DV/TV, whereas the branching density from the 2D carmine analysis showed only 1.5-fold increase. Another advantage of the microCT analysis is that through the measurement of the total tissue volume (TV), differences were identified among the distinct developmental stages [Fig. 3(c)] that could not be detected through the measurement of the total mammary area by the 2D carmine/Sholl analysis [Fig. 1(e)].

We further validated our microCT approach upon administration of a low dose of synthetic progesterone (MPA)[38,39,50–52] for a period of 4 days to 8-week-old female mice of the C57BL/6 genetic background, which is more resistant to MPA compared with other strains,[50] to capture small ductal changes. The effectiveness of the MPA treatment was confirmed by the increased expression of Cyclin D1 both at the mRNA and protein levels as well as by the increase of CK8+ cells, indicating proliferation of luminal cells. MicroCT analysis managed to detect an increase of the ductal volume and thickness upon MPA treatment that could not be traced by Sholl analysis (Fig. 4), indicating the usefulness of the various volumetric parameters used for the identification of ductal changes.

In conclusion, PTA-enhanced microCT constitutes a simple technique with short duration, high-resolution and possibility of recapitulating the 3D morphology of the mammary epithelium structure. Moreover, we provided a wide range of parameters, capable to perform volumetric analysis for the assessment of the complexity of mouse mammary epithelium at any developmental stage. Notably, even small structural alteration in the mammary duct tree were detectable, as shown by short treatment with MPA. Thus, PTA-enhanced microCT provides detailed and refined mammary gland tree anatomy that can be applied to morphological studies of mutant mouse models and for the preclinical evaluation of pharmaceuticals in breast cancer models.

Disclosure

The authors declare that they have no conflicts of interest.

Acknowledgments

We would like to thank the microCT facility at Biomedical Sciences Research Center "Alexander Fleming" for performing microCT scans. This research has been cofinanced by the European Union and Greek national funds through the Operational Program Competitiveness, Entrepreneurship, and Innovation under the call RESEARCH – CREATE – INNOVATE (Project code: T1EDK-02829).

References

1. C. J. Watson and W. T. Khaled, "Mammary development in the embryo and adult: a journey of morphogenesis and commitment," *Development* **135**(6), 995–1003 (2008).
2. C. W. Daniel and G. H. Smith, "The mammary gland: a model for development," *J. Mammary Gland Biol. Neoplasia* **4**(1), 3–8 (1999).

3. C. Brisken and D. Ataca, "Endocrine hormones and local signals during the development of the mouse mammary gland," *Wiley Interdiscip. Rev. Dev. Biol.* **4**(3), 181–195 (2015).
4. H. J. Lee et al., "Progesterone drives mammary secretory differentiation via RankL-mediated induction of Elf5 in luminal progenitor cells," *Development* **140**(7), 1397–1401 (2013).
5. R. Fernandez-Valdivia et al., "The RANKL signaling axis is sufficient to elicit ductal side-branching and alveologenesis in the mammary gland of the virgin mouse," *Dev. Biol.* **328**(1), 127–139 (2009).
6. S. McNally and T. Stein, "Overview of mammary gland development: a comparison of mouse and human," *Methods Mol. Biol.* **1501**, 1–17 (2017).
7. A. H. Fischer et al., "Hematoxylin and eosin staining of tissue and cell sections," *Cold Spring Harb. Protoc.* **2008**(5), 4986–4988 (2008).
8. D. K. Tucker et al., "Preparation of high-quality hematoxylin and eosin-stained sections from rodent mammary gland whole mounts for histopathologic review," *Toxicol. Pathol.* **44**(7), 1059–1064 (2016).
9. L. Tabár et al., "A new approach to breast cancer terminology based on the anatomic site of tumour origin: the importance of radiologic imaging biomarkers," *Eur. J. Radiol.* **149**, 110189 (2022).
10. S. Blacher et al., "Quantitative assessment of mouse mammary gland morphology using automated digital image processing and TEB detection," *Endocrinology* **157**(4), 1709–1716 (2016).
11. M. Montévil et al., "A combined morphometric and statistical approach to assess non-monotonicity in the developing mammary gland of rats in the clarity-BPA study," *Environ. Health Perspect.* **128**(5), 57001 (2020).
12. S. Preibisch, S. Saalfeld, and P. Tomancak, "Globally optimal stitching of tiled 3D microscopic image acquisitions," *Bioinformatics* **25**(11), 1463–1465 (2009).
13. S. B. Rasmussen, L. J. T. Young, and G. H. Smith, "Preparing mammary gland whole mounts from mice," in *Methods in Mammary Gland Biology and Breast Cancer Research*, M. M. Ip and B. B. Asch, Eds., pp. 75–85, Springer, Boston, Massachusetts (2000).
14. J. Schindelin et al., "Fiji: an open-source platform for biological-image analysis," *Nat. Methods* **9**(7), 676–682 (2012).
15. J. P. Stanko and S. E. Fenton, "Quantifying branching density in rat mammary gland whole-mounts using the Sholl analysis method," *J. Vis. Exp.* **2017**(125), 1–12 (2017).
16. J. N. McGinley and H. J. Thompson, "Quantitative assessment of mammary gland density in rodents using digital image analysis," *Biol. Proced. Online* **13**(1), 4 (2011).
17. J. P. Stanko, M. R. Easterling, and S. E. Fenton, "Application of Sholl analysis to quantify changes in growth and development in rat mammary gland whole mounts," *Reprod. Toxicol.* **54**, 129–135 (2015).
18. D. L. Hadsell et al., "In-silico QTL mapping of postpubertal mammary ductal development in the mouse uncovers potential human breast cancer risk loci," *Mamm. Genome.* **26**(1–2), 57–79 (2015).
19. S. D. Auweter et al., "X-ray phase-contrast imaging of the breast - advances towards clinical implementation," *Br. J. Radiol.* **87**(1034), 20130606 (2014).
20. S. T. Taba et al., "X-ray phase-contrast technology in breast imaging: principles, options, and clinical application," *Am. J. Roentgenol.* **211**(1), 133–145 (2018).
21. M. L. Bouxsein et al., "Guidelines for assessment of bone microstructure in rodents using micro-computed tomography," *J. Bone Miner. Res.* **25**(7), 1468–1486 (2010).
22. P. M. Gignac and N. J. Kley, "Iodine-enhanced micro-CT imaging: methodological refinements for the study of the soft-tissue anatomy of post-embryonic vertebrates," *J. Exp. Zool. Part B Mol. Dev. Evol.* **322**(3), 166–176 (2014).
23. K. Degenhardt et al., Rapid 3D phenotyping of cardiovascular development in mouse embryos by micro-CT with iodine staining," *Circ. Cardiovasc. Imaging* **3**(3), 314–322 (2010).
24. E. L. Scheller et al., "Use of osmium tetroxide staining with microcomputerized tomography to visualize and quantify bone marrow adipose tissue in vivo," *Methods Enzymol.* **537**, 123–139 (2014).

25. S. S. Karhula et al., "Effects of articular cartilage constituents on phosphotungstic acid enhanced micro-computed tomography," *PLoS One* **12**(1), e0171075 (2017).
26. C. J. Churukian, "Improved methods for staining fibrin," *J. Histotechnol.* **26**(2), 127–129 (2003).
27. A. Manlow and D. G. Munoz, "A non-toxic method for the demonstration of gliosis," *J. Neuropathol. Exp. Neurol.* **51**(3), 298–302 (1992).
28. B. D. Metscher, "Micro CT for comparative morphology: simple staining methods allow high-contrast 3D imaging of diverse non-mineralized animal tissues," *BMC Physiol.* **9**(1), 11 (2009).
29. B. D. Metscher, "MicroCT for developmental biology: a versatile tool for high-contrast 3D imaging at histological resolutions," *Dev. Dyn.* **238**(3), 632–640 (2009).
30. P. J. Dunmore-Buyze et al., "Three-dimensional imaging of the mouse heart and vasculature using micro-CT and whole-body perfusion of iodine or phosphotungstic acid," *Contrast Media Mol. Imaging* **9**(5), 383–390 (2014).
31. K. M. Lesciotto et al., "Phosphotungstic acid-enhanced microCT: optimized protocols for embryonic and early postnatal mice," *Dev. Dyn.* **249**(4), 573–585 (2020).
32. G. Fiorentino et al., "Three-dimensional micro-computed tomography of the adult mouse ovary," *Front. Cell Dev. Biol.* **8**, 1–8 (2020).
33. J. Missbach-Guentner et al., "3D virtual histology of murine kidneys-high resolution visualization of pathological alterations by micro computed tomography," *Sci. Rep.* **8**(1), 1407 (2018).
34. E. Douni et al., "A RANKL G278R mutation causing osteopetrosis identifies a functional amino acid essential for trimer assembly in RANKL and TNF," *Hum. Mol. Genet.* **21**(4), 784–798 (2012).
35. V. Rinotas et al., "Novel genetic models of osteoporosis by overexpression of human RANKL in transgenic mice," *J. Bone Miner. Res.* **29**(5), 1158–1169 (2014).
36. J. Shu et al., "Statistical colour models: an automated digital image analysis method for quantification of histological biomarkers," *Biomed. Eng. Online* **15**(1), 1–16 (2016).
37. J. W. Fuseler et al., "Morphometric and fractal dimension analysis identifies early neoplastic changes in mammary morphometric and fractal dimension analysis epithelium of MMTV-cNeu mice JOHN," *Anticancer Res.* **34**(3), 1171–1177 (2014).
38. C. Otto et al., "Comparative analysis of the uterine and mammary gland effects of drospirenone and medroxyprogesterone acetate," *Endocrinology* **149**(8), 3952–3959 (2008).
39. C. E. Wood et al., "Progestin effects on cell proliferation pathways in the postmenopausal mammary gland," *Breast Cancer Res.* **15**(4), R62 (2013).
40. F. S. Kittrell et al., "Prospective isolation and characterization of committed and multipotent progenitors from immortalized mouse mammary epithelial cells with morphogenic potential," *Breast Cancer Res.* **13**(2), R41 (2011).
41. C. S. Atwood et al., "Progesterone induces side-branching of the ductal epithelium in the mammary glands of peripubertal mice," *J. Endocrinol.* **167**(1), 39–52 (2000).
42. M. Bech et al., "In-vivo dark-field and phase-contrast x-ray imaging," *Sci. Rep.* **3**, 10–12 (2013).
43. F. Palermo et al., "X-ray phase contrast tomography serves preclinical investigation of neurodegenerative diseases," *Front. Neurosci.* **14**, 1–11 (2020).
44. S. De Bournonville, S. Vangrunderbeeck, and G. Kerckhofs, "Contrast-enhanced microCT for virtual 3D anatomical pathology of biological tissues: a literature review," *Contrast Media Mol. Imaging* **2019**, 8617406 (2019).
45. P. Vickerton, J. Jarvis, and N. Jeffery, "Concentration-dependent specimen shrinkage in iodine-enhanced microCT," *J. Anat.* **223**(2), 185–193 (2013).
46. A. C. Lendrum et al., "Studies on the character and staining of fibrin," *J. Clin. Pathol.* **15**, 401–413 (1962).
47. M. Doube et al., "BoneJ: free and extensible bone image analysis in ImageJ," *Bone* **47**(6), 1076–1079 (2010).
48. A. Popov et al., "Astrocyte dystrophy in ageing brain parallels impaired synaptic plasticity," *Aging Cell* **20**(3), 1–14 (2021).

49. W. Xiong et al., "Notch3 knockout suppresses mouse mammary gland development and inhibits the proliferation of 4T1 murine mammary carcinoma cells via CCL2/CCR4 axis," *Front. Cell Dev. Biol.* **8**, 594372 (2020).
50. G. Montero Girard et al., "Association of estrogen receptor-α and progesterone receptor A expression with hormonal mammary carcinogenesis: role of the host microenvironment," *Breast Cancer Res.* **9**(2), R22 (2007).
51. L. Wan et al., "MTDH-SND1 interaction is crucial for expansion and activity of tumor-initiating cells in diverse oncogene- and carcinogen-induced mammary tumors," *Cancer Cell* **26**(1), 92–105 (2014).
52. J. L. Schwartz-Roberts et al., "Interferon regulatory factor-1 signaling regulates the switch between autophagy and apoptosis to determine breast cancer cell fate," *Cancer Res.* **75**(6), 1046–1055 (2015).

Anthi Kolokotroni received her BSc degree in chemistry from the University of Patras, Greece, in 2014 and her MSc diploma degree in applied biochemistry from the same department where she focused on the role of proteoglycans in breast cancer. In June 2017, she joined Prof. Eleni Douni's laboratory, at Biomedical Sciences Research Center "Alexander Fleming," where she started her doctoral studies studying the role of RANKL in mammary gland pathophysiology using transgenic mouse models.

Evi Gkikopoulou received her diploma degree at the Department of Biotechnology in School of Applied Biology and Biotechnology in Agricultural University of Athens (integrated master), Greece, in 2019. In December 2019, she joined Prof. Eleni Douni's laboratory at the Institute for Bioinnovation of Biomedical Sciences Research Center "Alexander Fleming," where she started her doctoral studies investigating mechanisms of carcinogenesis in transgenic mice overexpressing human RANKL.

Vagelis Rinotas obtained his PhD at the Department of Biotechnology in School of Applied Biology and Biotechnology in Agricultural University of Athens, Greece, in 2014. In 2015 to 2022, as a Postdoc Fellow at Dr. Douni's laboratory, at the Institute for Bioinnovation of Biomedical Sciences Research Center "Alexander Fleming," he studied the pathophysiological role of RANKL in osteoporosis, bone marrow adiposity, and breast cancer.

Eleni Douni received her BSc and PhD degrees from the Biology Department of the University of Athens, Greece, trained in mouse genetic engineering through the generation and analysis of transgenic mice as models of human diseases. Currently, she is working as a professor in the Laboratory of Genetics of the Biotechnology Department at the Agricultural University of Athens and is Associate Researcher at the Institute for Bioinnovation of Biomedical Sciences Research Center "Alexander Fleming."